Metabolic connectomics targeting brain pathology in dementia with Lewy bodies

Silvia P Caminiti[1,2,*], Marco Tettamanti[2,3,*], Arianna Sala[2,*],
Luca Presotto[2], Sandro Iannaccone[4], Stefano F Cappa[2,5],
Giuseppe Magnani[6] and Daniela Perani[1,2,3] for
the Alzheimer's Disease Neuroimaging Initiative (ADNI)

Abstract

Dementia with Lewy bodies is characterized by α-synuclein accumulation and degeneration of dopaminergic and cholinergic pathways. To gain an overview of brain systems affected by neurodegeneration, we characterized the [18F]FDG-PET metabolic connectivity in 42 dementia with Lewy bodies patients, as compared to 42 healthy controls, using sparse inverse covariance estimation method and graph theory. We performed whole-brain and anatomically driven analyses, targeting cholinergic and dopaminergic pathways, and the α-synuclein spreading. The first revealed substantial alterations in connectivity indexes, brain modularity, and hubs configuration. Namely, decreases in local metabolic connectivity within occipital cortex, thalamus, and cerebellum, and increases within frontal, temporal, parietal, and basal ganglia regions. There were also long-range disconnections among these brain regions, all supporting a disruption of the functional hierarchy characterizing the normal brain. The anatomically driven analysis revealed alterations within brain structures early affected by α-synuclein pathology, supporting Braak's early pathological staging in dementia with Lewy bodies. The dopaminergic striato-cortical pathway was severely affected, as well as the cholinergic networks, with an extensive decrease in connectivity in Ch1-Ch2, Ch5-Ch6 networks, and the lateral Ch4 capsular network significantly towards the occipital cortex. These altered patterns of metabolic connectivity unveil a new in vivo scenario for dementia with Lewy bodies underlying pathology in terms of changes in whole-brain metabolic connectivity, spreading of α-synuclein, and neurotransmission impairment.

Introduction

Dementia with Lewy bodies (DLB) is the second most common neurodegenerative dementia, characterized by a progressive and fluctuating cognitive decline, variably accompanied by extrapyramidal features, rapid eye movement sleep behavior disorder (RBD), and visual hallucinations.[1]

DLB is linked to a disturbance of protein metabolism, producing an abnormal accumulation of α-synuclein in the brain.[2,3] It has been proposed that α-synuclein diffuses following a prion-like mechanism causing synaptic dysfunctions, and progressive neuronal death.[4,5] Braak et al.[6,7] formalized the topographical progression of α-synuclein pathology in Parkinson's disease (PD) and

[1]Vita-Salute San Raffaele University, Faculty of Medicine and Surgery, Milan, Italy
[2]Division of Neuroscience, San Raffaele Scientific Institute, Milan, Italy
[3]Nuclear Medicine Unit, San Raffaele Hospital, Milan, Italy
[4]Neurological Rehabilitation Department, San Raffaele Hospital, Milan, Italy
[5]IUSS Pavia, Piazza della Vittoria, Pavia, Italy
[6]Department of Neurology, San Raffaele Hospital, Milan, Italy

*These authors contributed equally to this work.

Corresponding author:
Daniela Perani, Division of Neuroscience, San Raffaele Scientific Institute, Nuclear Medicine Unit, Vita-Salute San Raffaele University, San Raffaele Hospital, Via Olgettina 60, Milan 20132, Italy.
Email: perani.daniela@hsr.it

DLB, from brainstem to neocortical structures, among cells sharing common features.

Accumulation of α-synuclein is the key event causing synaptic dysfunction and leading to neurodegenerative symptoms in both DLB and PD.[8] The link between pathology and neurodegeneration is mediated by the *metabolic* pathways involved in neuronal function and bioenergetics.[9–12] In DLB there is consistent evidence for a specific dysfunctional pattern, characterized by widespread reductions of metabolism in occipital, parieto-temporal and, to a lesser extent, frontal cortex, supportive for clinical diagnosis.[1,13]

The neurodegeneration of dopaminergic and cholinergic neurotransmission systems is a relevant aspect in DLB pathogenesis, as shown by *post-mortem*[14–16] and in vivo[17,18] brain studies, and is the basis for the major clinical features.[1] The accumulation of α-synuclein is associated with cholinergic,[14,19] and nigrostriatal dopaminergic[8,20] deficits.

Specific brain circuits, as shown in functional magnetic resonance imaging (fMRI) studies, are disrupted in the different neurodegenerative conditions, in keeping with the principle of selective neuronal vulnerability, according to which specific neuronal populations die, whereas other are resistant to neurodegeneration.[21] Previous fMRI studies of brain connectomics in neurodegenerative diseases, showed a reduced connectivity in the default mode network (DMN) in Alzheimer's Disease (AD), whereas the behavioral variant of fronto-temporal dementia has been associated to a disruption of the anterior salience network. An impairment of thalamo-cortical and cerebellar-thalamo-cortical networks was also reported in PD and in progressive sopranuclear palsy, respectively.[22] A functional network perspective was also adopted in some fMRI studies in DLB showing mixed results regarding DLB connectivity profiles.[23–28] [18F]FDG-PET was recently applied to the study of metabolic connectivity (MC) identifying disease-specific patterns of alterations consistent with the underlying pathology.[29–31] [18F]FDG-PET is considered an index of integrated local synaptic activity,[12] and its signal has also been associated to synaptic density and function.[10,11] It is thus considered a unique tool for capturing the heterogeneous events that contribute to synaptic dysfunction in neurodegenerative diseases, such as altered intracellular signaling cascades, impaired neurotransmitter release, spreading of proteinopathies, and long-distance disconnection.[9]

Studying neurodegenerative diseases with a metabolic network perspective might thus provide important insights into the link between local vulnerabilities, long-range disconnection, and the effects of neuropathology.

The investigation of brain MC is based on the assumption that regions whose metabolism is correlated are functionally interconnected.[32] This assumption has its foundations in a pioneering study, in which Horwitz et al.[32] explored brain MC in healthy subjects, demonstrating that the results are largely consistent with known anatomo-functional data. Recent evidence indicates a close relationship between resting state functional brain connectivity (rs-fMRI), and glucose consumption, as measured by [18F]FDG-PET.[33,34] Passow et al.[33] found spatial similarities between local glucose and BOLD signal fluctuations. Both fluctuations also correlated with DMN functional connectivity. Their findings suggest a close relationship between BOLD signal fluctuations, functional connectivity, and cerebral metabolism.[33]

Riedl et al.[34] simultaneously acquired fMRI and [18F]FDG-PET data for obtaining a novel measure suitable to calculate brain state effective connectivity. The integrated brain metabolic [18F]FDG-PET with fMRI data provided directionality of brain signaling, since increases in local metabolism reflect an increase in afferent effective connectivity.

The above studies combining metabolic and functional connectivity approaches support the integrated value of the two modalities.[33,34]

Crucially, no study has hitherto characterized the whole-brain and anatomically oriented MC in DLB using [18F]FDG-PET. Although fMRI can incorporate the time series from individual subjects, thus increasing the statistical power over a single time point per subject as required for [18F]FDG-PET data, specific methods have been adopted for PET metabolic data.[35–37] Specifically, here we used the sparse inverse covariance estimation (SICE) method, allowing reliable estimation of inverse covariance for [18F]FDG-PET data with relatively small sample size.[35] Here, we aimed at identifying the brain MC changes in DLB that can shed light on the relationship between synaptic dysfunctions and the underlying pathology associated to DLB.[21,38] We thus tested a comprehensive model for altered brain connectivity in DLB, by considering MC in the whole-brain and in neurotransmission pathways, following the increasing evidence that functional connectivity and network metabolic activity are sensible to changes in neurotransmission.[39,40] We focused on the dopaminergic and cholinergic systems in order to explore the effects on metabolic disconnections and connectivity reconfiguration in each of these pathways, which represent the major biochemical neuropathology. In addition, we analyzed MC of brain regions affected by α-synuclein spreading, with the aim to in vivo explore and support the Braak et al.'s[6,7] staging hypothesis to DLB condition.

Materials and methods

Data used in the preparation of this article were obtained from the Alzheimer's Disease Neuroimaging Initiative (ADNI) database (adni.loni.usc.edu). The ADNI was launched in 2003 as a public–private partnership, led by Principal Investigator Michael W. Weiner, MD. The primary goal of ADNI has been to test whether serial magnetic resonance imaging (MRI), positron emission tomography (PET), other biological markers, and clinical and neuropsychological assessment can be combined to measure the progression of mild cognitive impairment (MCI) and early AD. For up-to-date information, see www.adni-info.org.

Subjects

DLB patients were retrospectively collected from the clinical and imaging database of the San Raffaele Hospital, Milan. Expert neurologists performed the final diagnosis, considering full neurological information and follow-up, neuropsychological assessment, CT or MRI, [18F]FDG-PET scans and the CSF measures. Patients showing cerebrovascular abnormalities on MRI or CT were excluded from the analyses.

As supporting information for the diagnosis, we used a [18F]FDG-PET Statistical Parametrical Mapping (SPM) t-map comparing each individual with a standardized healthy control (HC) group,[41] and we specifically looked for the pattern of hypometabolism in the medial and/or lateral occipital cortex, which is considered the hallmark of DLB, accompanied by temporo-parietal and frontal cortex hypometabolism[1,41,42] (see Supplementary Figure S1).

According to the diagnosis at the clinical follow-up, we identified 42 out of 83 patients fulfilling consensus criteria for DLB,[1] and not showing any neurological and psychiatric comorbidities. The group of patients was composed of 27 males and 15 females, with a mean age $\pm$ SD of 72.26 ± 6.74 years; 71.43% of DLB patients presented parkinsonism, 64.29% RBD, and 59.52% visual hallucinations. The DLB group had a mean disease duration $\pm$ SD of 2.14 ± 1.4 years.

We selected 35 HC subjects from the control database of Nuclear Medicine Unit, San Raffaele Hospital, Milan. In order to obtain equal sample size with the DLB group and to avoid inter-scanner variability, we added seven FDG PET images from the ADNI database (adni.loni.usc.edu). The final group of 42 HC comprised 22 males and 20 females, matched for age, with a mean age $\pm$ SD of 72.10 ± 5.93 years. Age and gender between DLB and HC groups did not differ (F = 0.14, $p = 0.906$; $\chi^2 = 1.224$, $p = 0.268$).

HC and DLB patient studies performed in Milan were approved by the San Raffaele Hospital Medical Ethics Committee. Both groups provided written informed consent, following detailed explanation of each experimental procedure. ADNI controls gave written informed consent at the time of enrolment for data collection and completed questionnaires approved by each participating sites Institutional Review Board.

The protocols conformed to the ethical standards of the Declaration of Helsinki for protection of human subjects.

[18F]FDG-PET image acquisition and reconstruction

The [18F]FDG-PET scans of the 42 DLB patients and 42 HC were acquired using the same Discovery STE PET (3.27-mm thickness; in-plane FWHM 5.55-mm) manufactured by GE Healthcare.

The 77 (35 HC and 42 DLB) [18F]FDG-PET acquisitions performed at the Nuclear Medicine Unit, San Raffaele Hospital conformed to the European Association of Nuclear Medicine guidelines.[43] Static emission images were acquired 45-min after injecting 185–250 MBq of [18F]FDG via a venous cannula. This post-injection time interval allows to obtain an equal distribution of the tracer across the entire brain, with negligible blood flow-dependent differences, thus achieving an optimal signal-to-noise ratio.[44] The duration of scan acquisition was of 15 min.

The seven steady-state emission images obtained from the ADNI dataset were acquired 30 min after injecting approximately 185MBq of [18F]FDG via a venous cannula, with scan acquisition duration of 30 min. After realignment to correct for eventual interframe motion, the last three frames lasting 5 min each were combined to obtain a single 15-min static image representing the distribution during the whole acquisition time. In this way, the uptake time of ADNI images was uniformed to that of San Raffaele images.

In this study, uniform reconstruction protocols were applied, in particular, the use of the ordered subset-expectation maximization algorithm and CT attenuation correction procedures. A rigorous quality control process was performed to check for major artefacts in PET raw images, including defective image uniformity and orientation, or attenuation correction due to a mismatch between CT and PET images.

Metabolic connectomics

[18F]FDG-PET image pre-processing. All scans underwent general pre-processing procedures, using the MATLAB (http://it.mathworks.com/products/matlab/) (Mathworks Inc., Sherborn, Mass., USA) based

software SPM5 (http://www.fil.ion.ucl.ac.uk/spm/soft ware/SPM5/). In details, each image was first normalized to a [18F]FDG-PET specific template registered to the Montreal Neurological Institute (MNI) standard space, developed by our group,[45] using the default SMP5 bounding-box, and with an isotropic voxel size of 2 mm. The specific [18F]FDG-PET template provides high levels of normalization accuracy, and it reduces random effects due to noise.[45] All the normalized PET images were spatially smoothed with an 8 mm isotropic 3D Gaussian FWHM kernel. Moreover, every image was proportionally scaled to its global mean,[46] in order to account for between-subject uptake variability,[47] thus obtaining higher signal-to-noise ratio compared to other available scaling methods (e.g. cerebellar reference area).[48]

Node selection and ROIs definition

We created the *whole-brain MC matrix* (i.e. the full-matrix), considering cortical, subcortical, cerebellar, and brainstem regions (121 × 121 ROIs), with the objective to cover the whole-brain structures. These regions represented the basic units of the network, i.e. the nodes. There were 92 nodes for cortical and subcortical structures, 26 nodes for the cerebellum, and 3 nodes for brainstem (Supplementary Table S1A).

Moreover, another analysis was performed according to Huang et al.,[35] and subdividing the full-matrix into 12 sub-matrices, representative of larger brain regions (see Supplementary Table S1B).

In addition, we performed a set of spatially anatomically driven connectivity analyses, addressing neural networks related to DLB pathology. These included the cholinergic[49–51] and dopaminergic[52,53] neurotransmission systems, as well as the spreading of α-synuclein accumulation in the brain according to Braak et al.'s[6,7] stages progression.

As for the α-synuclein analysis, we considered Braak et al.[6] stages one to four. Braak et al.'s[7] staging was originally proposed for PD and subsequently also for DLB, supported by evidence showing consistent data in the spreading of α-synuclein pathology.[54,55] We constructed the α-synuclein network considering medulla oblongata and pons, for stages one to two, midbrain, hippocampus, parahippocampal gyrus, ventral striatum, and amygdala for stages three to four.[6] Medulla and pons contain gray matter nuclei early affected by α-synuclein pathology, i.e. the dorsal IX-X motor nuclei, intermediate reticular zone, caudal raphe nuclei, gigantocellular reticular nucleus, and coeruleus/subcoeruleus complex[6] (Supplementary Table S2).

Concerning the *dopaminergic system* anatomically driven analysis, we created two different networks representing the striato-cortical and meso-limbic

pathways. The striato-cortical network consisted of dorsal caudate and dorsal putamen, frontal premotor, motor, executive dorsolateral frontal regions, and somatosensory cortex; the meso-limbic network consisted of ventral striatum, ventral and medial frontal areas, anterior and middle cingulate cortices, as well as the amygdala and parahippocampal cortex[52,53] (Supplementary Table S3).

For the *cholinergic system analysis*, we considered six different cholinergic pathways.[49–51] The first network consisted of the brain regions innervated by Ch1 and Ch2 nuclei of the forebrain, namely the bilateral hippocampus and hypothalamus. The second network represented the pathway arising from Ch3 nucleus, that reach the olfactory and parahippocampal cortices. The third, fourth, and fifth cholinergic networks were represented by the pathways originating from Ch4 nuclei. Namely, the third Ch4 medial pathway reaches cingulate, retrosplenial, and orbitofrontal cortices; the fourth Ch4 lateral perisylvian division joints olfactory and superior temporal cortices, plus the insula and the fronto-parietal operculum; the fifth Ch4 lateral capsular division supplies the remaining frontal, parietal, temporal, and occipital cortices, as well as the amygdala. The cholinergic nuclei of the brainstem, i.e. the Ch5 pedunculopontine tegmental nucleus and the Ch6 laterodorsal tegmental gray of periventricular area, reach the thalamus, ventral and dorsal striatum, globus pallidus, and the brainstem reticular formation represented by pons, midbrain, and medulla oblongata (Supplementary Table S4).

In all the aforementioned pathways, we excluded the small output nuclei from which each molecular network originates (i.e. substantia nigra, ventrotegmental area, and Ch1, 2, 3, 4, 5, 6 nuclei), due to the limited spatial resolution of PET method and the lack of reference atlases for these regions.

All the ROIs used for the connectivity analyses were derived from AAL atlas,[56] with the following exceptions: (i) for the hypothalamus, we created spherical ROIs with a 5-mm radius centered at [±8 −4 −4] MNI coordinates, according to Kroemer et al.;[57] (ii) for the brainstem, we used ROIs available in WFUPickAtlas Tailarach Daemon Lobar Atlas; (iii) for the dorsal and ventral striatum, ROIs were manually drawn in MriCron (www.mricro.com), using a standard high-resolution MRI T1 image as anatomical template, in accordance to the structural subdivision of the basal ganglia proposed by Tziortzi et al.[58]

Furthermore, prior to the analyses, we verified that the volume of each ROI included was not smaller than three times the FWHM of the scanner spatial resolution. This spatial resolution cut-off is considered to be the lower limit to avoid confounding effects such as

blurring or spill-over (i.e. ROI partial volume effects).[59,60]

Construction of brain connectivity matrices. We created whole-brain, dopaminergic, cholinergic, and α-synuclein Subject-by-Node/ROI matrices for each group (HC, DLB). The matrices contained the regional cerebral metabolic values derived from each subject in each node/ROI. To obtain the MC matrices, we used the SICE method.[35] This method has been previously used in other [18F]FDG-PET studies, since it allows reliable estimation of inverse covariance even with sample sizes equal or even smaller than the number of nodes selected. This is crucial as in [18F]FDG-PET studies the sample size is the number of subjects and not the length of the time series, as in fMRI studies.[35] In order to apply SICE, we verified that data followed a multivariate normality distribution. Even though multivariate normality of cerebral metabolism data is usually assumed a priori,[35] we nevertheless verified it performing a Mardia test. Since the number of variables (i.e. nodes) was greater than the number of cases, we performed multiple multivariate normality tests on smaller random subsamples of nodes, so that the assumptions for the application of Mardia test were fulfilled. We found that both [18F]FDG-PET metabolic data of HC and DLB followed a multivariate normality distribution.

Using the GraphVar toolbox,[61] we obtained unweighted binary MC matrices from Subject-by-Node matrices. Unweighted binary MC matrices consist of zero and non-zero entries, respectively, indicating the presence and absence of a significant partial correlation between two nodes (i.e. a functional connection between the two nodes).[62] We computed MC matrices with different densities, representing different numbers of connections. As there is no gold standard for the number of connections to be selected,[63] we considered matrices with three different numbers of connections that were proportional to the total number of nodes. For the whole-brain and cholinergic analyses, we used matrices with 200–400–600 connections. Given the smaller total number of nodes in the other anatomically driven analyses, we set matrices with 60–120–180 connections for the dopaminergic system and matrices with 10–20–30 connections for the α-synuclein network. Unweighted matrices were used for statistical testing, as reported below. Note that we set the number of connections to be the same for both groups. Setting a fixed threshold for both groups is a common strategy to compare the organization of connectivity between different groups, factoring out global connectivity differences (see Huang et al.[35]).

For each group, a summary whole-brain *semi-weighted* matrix was also obtained by summing up the

three unweighted binary matrices with 200–400–600 connections. The same procedure was applied to the binary matrices for dopamine, acetylcholine, and α-synuclein, in order to obtain semi-weighted matrices for each atlas at the three different densities. Note that when SICE is applied, the weight of the connections has to be interpreted as an ordinal measure.[35] Therefore, a single semi-weighted matrix containing "a-quasi measure" of strength (from 1 = lowest strength to 3 = highest strength) was obtained for each DLB and HC group. Semi-weighted matrices do not provide numerical information on the strength of connections, but a useful visual representation of the distribution of connections according to their strength level. Semi-weighted and unweighted MC matrices were represented in a 3D brain template using BrainNet toolbox (https://www.nitrc.org/projects/bnv/).[64]

Graph theory analyses. For the whole-brain full-matrix, we performed both a complex brain network analysis and a nodal analysis, using a set of functional connectivity indices.[65] For these analyses, we only considered the highest density network with 600 connections, in order to extract the best characteristic indices of network organization (see Seo et al.[63]). We computed average clustering coefficient (C) and modularity (Q) as measures of network segregation. A segregated network is characterized by the presence of densely interconnected groups of brain regions with specialized processing functions.[65,66] Global efficiency (E) and characteristic path length (L) were calculated as measures of network integration, accounting for the coordinate activity of distributed brain regions.[65,66] We also considered the small-worldness (S) index, representing the relationship between segregation and integration.[65] S was computed adopting the formula $S = (C/C_{rand})/(L/L_{rand})$.[65] C_{rand} and L_{rand} correspond to the mean clustering coefficient and mean characteristic path length, which were calculated based on 5000 randomly generated networks, all with the same degree distribution as the actually observed whole-brain network. Furthermore, we applied a data-driven subdivision of the network into modules (i.e. separated and non-overlapping sets of regions that are strongly connected to each other, and for this reason form independent modules), using the Louvain method.[65] If single-region modules were obtained, they were excluded from further analysis.

As for the nodal analysis, we computed the participation coefficient of each node[65] (See Supplementary Figure S2 for results relative to further nodal measures). The most important nodes of the network, i.e. the hubs, were identified. Hubs were computed by selecting nodes whose participation coefficient was one standard deviation higher than the mean

participation coefficient. The participation coefficient is an established index for hub identification and it has been proven to be more appropriate than other indices, as degree, at least for functional networks.[67]

Considering the sub-matrix based analysis, we calculated the total number of *within* or short-distance connections (i.e. connections linking two nodes in the same sub-matrix) and the total number of *between* or long-distance connections (i.e. connections linking two nodes belonging to different sub-matrices).

For the anatomically driven networks, we computed the total number of connections and nodal degree *within* each network.

In order to rigorously test whether differences between DLB and HC were significant, we adopted a bootstrap procedure,[35] allowing hypothesis testing when the sample size is not so large to produce statistical inference. For each connectivity matrix, we extracted 5000 bootstrap samples of 42 subjects, with replacement, both for DLB and HC.

For each of the 5000 bootstrap samples, we calculated global and local MC indices and number of connections within and between sub-matrices or networks. We then performed multiple independent t-tests, using a Bonferroni correction. We tested global indices for each network and local indices for each node identified as a hub. We also compared the number of connections for each of the 10 sub-matrices in the whole-brain analysis, and for each network in the molecular network analyses.

Since the main results were consistent across matrices with different numbers of connections, we only reported the results relative to the most conservative threshold (i.e. 200 connections for the whole-brain analysis, 10 for α-synuclein analysis, 60 for dopamine systems analysis, and 200 for cholinergic systems analysis).

Results

Whole-brain connectivity

Global measures. Segregation measures, i.e. clustering coefficient and modularity, were significantly decreased in DLB versus HC groups. As for integration measures, global efficiency increased, whereas characteristic path length decreased. Small-worldness was higher than 1 for both DLB and HC.

Number of connections. DLB connectivity matrices showed a marked whole-brain MC reconfiguration, characterized by an increase of long-distance and a reduction of local connections (Figure 1; Supplementary Table S5).

Modularity. The Louvain modularity method identified six modules for HC and eight modules for DLB. In DLB, the nodes were sparsely relocated across modules with respect to HC, with extensive reconfigurations in frontal lobes, including the orbitofrontal cortex, in the parietal and occipital lobes, and in cerebellum (Figure 2(a), for nodes and module reconfiguration).

Hubs. According to graph theory, we identified 21 hubs for the HC group and 9 hubs for DLB. In DLB compared to HC, the hubs were classified into three categories, i.e. lost, preserved, and reconfigured hubs. The hubs changes were consistent with the whole network reorganization, described above. Notably, the lost and reconfigured hubs were part of frontal, parietal, occipital, thalamic, and cerebellar regions (Figure 2(b)).

Sub-matrix connectivity

Number of connections. As for the sub-matrix-based analysis, we found significant local connectivity decreases within a number of sub-matrices, namely in the occipital cortex, the cerebellum, thalamus, and brainstem. There were in addition significant local connectivity increases within the parietal, temporal, and frontal sub-matrices, as well as in the basal ganglia.

Regarding long-distance connections, we found significant disconnections in sub-matrices that also showed local alterations. In the frontal sub-matrix, we found decreased connectivity with occipital and cerebellum sub-matrices, but enhanced connectivity with parietal and basal ganglia sub-matrices; the thalamus presented widespread disconnections with occipital cortex, median-cingulum, paracentral lobule, cerebellar, and brainstem sub-matrices. The cerebellum showed selective decreases in connectivity with frontal, occipital, thalamic, and brainstem sub-matrices (Figure 1(b); Supplementary Table S6).

Anatomically driven analysis

Alpha-synuclein spreading. Connectivity analysis of α-synuclein Braak et al.'s stages showed altered connectivity in regions corresponding to stages 1 to 4 (Figure 3). In particular, the projection from brainstem to hippocampal structures and amygdala were functionally disconnected.

The connectivity followed a specific gradient, characterized by a prevalent impairment in the brainstem regions, which following the Braak's hypothesis, represent the first regions to be affected. This result was consistent with the short disease duration of our sample.

Dopaminergic networks. A severe loss of connections from dorsal striatum to the prefrontal, sensorimotor cortex, and the supplementary motor region characterized DLB. This network displayed highly
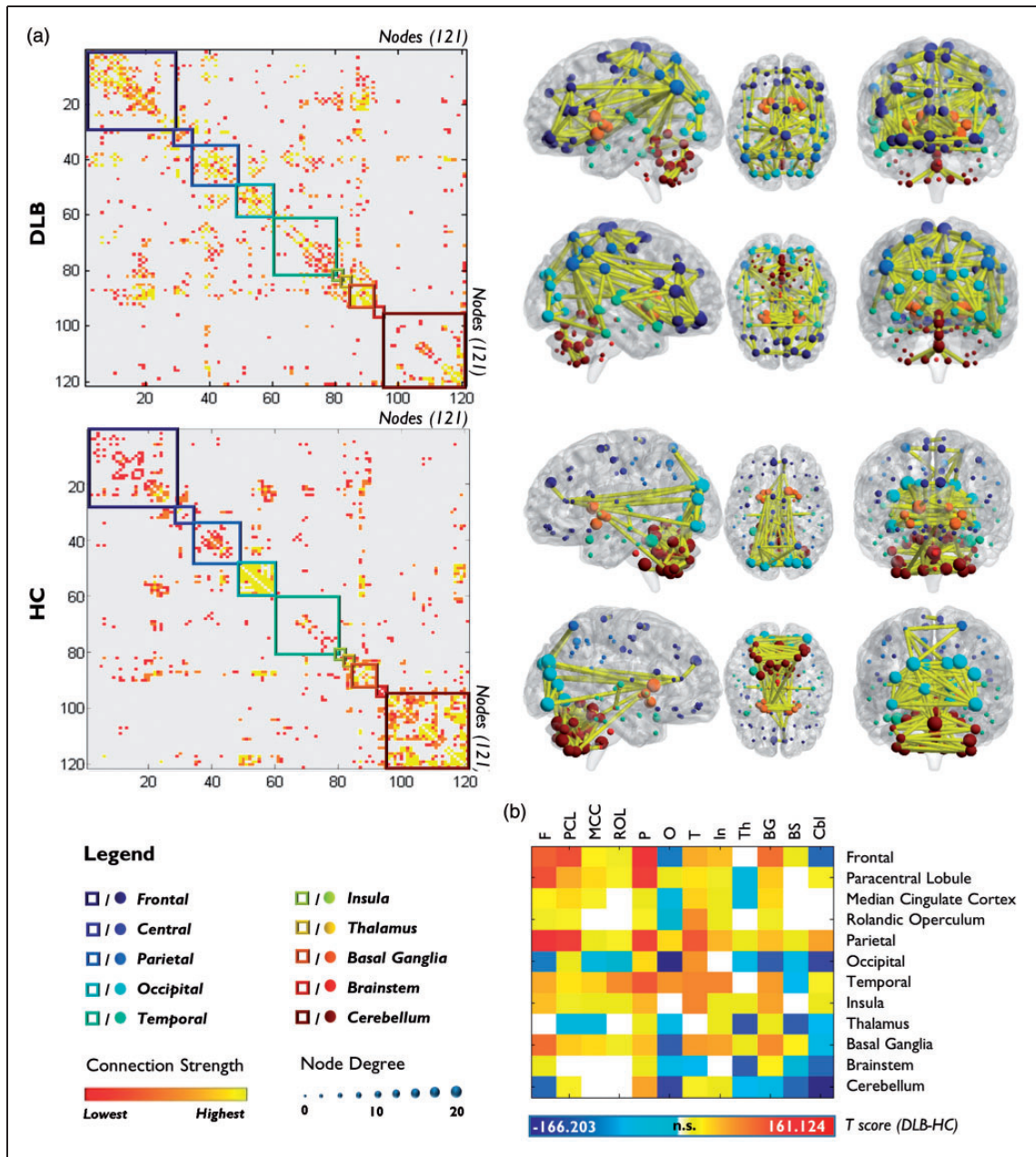
Figure 1. Whole-brain metabolic connectome in DLB and HC. (a) The first column displays correlation matrices of DLB and HC obtained from the analysis of the full-matrix composed by 121 nodes. The red-yellow color gradient represents the weight of the correlation between nodes, whereas colored squares indicate the nodes' anatomical localization. The second column displays DLB and HC brain connectivity graphs on a 3D brain template. Only the strongest connections are presented (in yellow). The dimension of each node depends on the node total number of connections, whereas the color indicates its anatomical localization. A global connectivity derangement and reconfiguration is evident in DLB versus HC, with the pathological group showing a loss of the hierarchical functional skeleton found in healthy subjects. (b) The T-score matrix shows differences in the number of connections within and between each sub-matrix in DLB versus HC.

F: frontal; PCL: paracentral lobule; MCC: median cingulate cortex; ROL: rolandic operculum; P: parietal; O: occipital; T: temporal; In: insula; Th: thalamus; BG: basal ganglia; BS: brainstem; Cbl: cerebellum.

interconnected nodes in HC. Differently, meso-limbic network connectivity remained more spared, with limited loss of connectivity from the ventral striatum (Figure 4; Supplementary Table S7).

Cholinergic networks. A diffuse reconfiguration, characterized by both increased and decreased connectivity, was found in cholinergic networks (Figure 5). Specifically, Ch1-Ch2 and Ch5-Ch6 cholinergic

networks showed decreases in the number of connections. Specifically, the Ch1-Ch2 network, hypothalamic regions were the most affected, together with the thalamic, midbrain, and pontine regions within the

Figure 2. Modules and hubs. (a) Modular subdivision of DLB and HC whole-brain networks, performed with Louvain modularity method. An overall poorly delineated modular organization is present in DLB. (b) Hub reconfiguration in DLB. Blue circles represent lost hubs (hubs present in HC but not in DLB); green circles indicate preserved hubs (hubs present in both DLB and HC); red circles show reconfigured hubs (nodes that in DLB assume the role of hubs differently to HC).
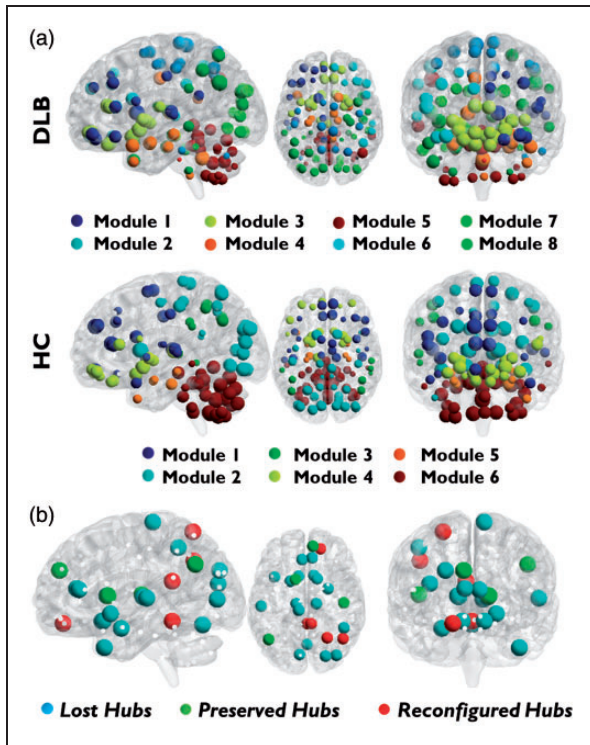
Ch5-Ch6 network. In contrast, Ch3 and the lateral Ch4 perisylvian division networks presented with a global reconfiguration and connectivity increases between nodes. The medial and the lateral capsular Ch4 nuclei pathways showed a mixed profile, characterized by both increases and decreases in connectivity. Namely, the medial Ch4 showed a slight decrease in the number of connections to anterior and median cingulate regions, and an increase to the orbital regions and posterior cingulate gyrus. The lateral Ch4 capsular division showed decreased connectivity to the occipital lobe and, to a lesser extent, to the frontal superior medial regions, and a strong increase in the number of connections to the parietal lobe, notably the angular gyri (Supplementary Table S8).

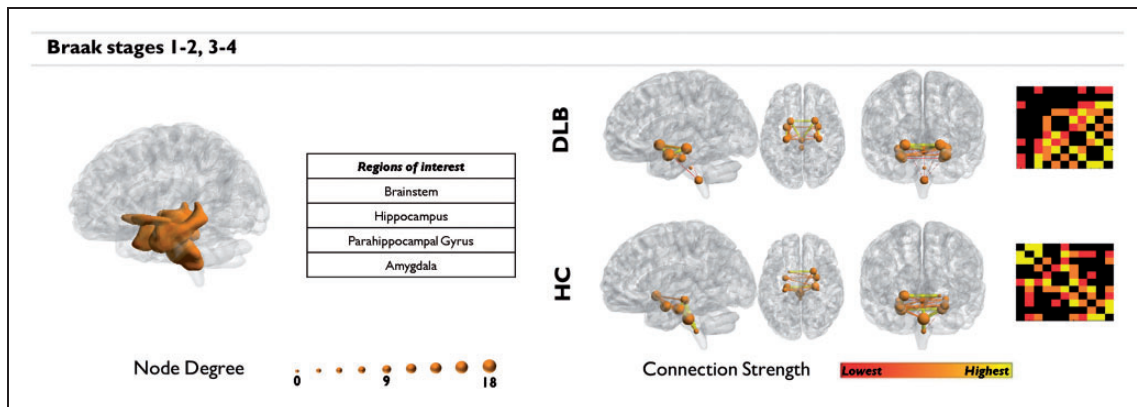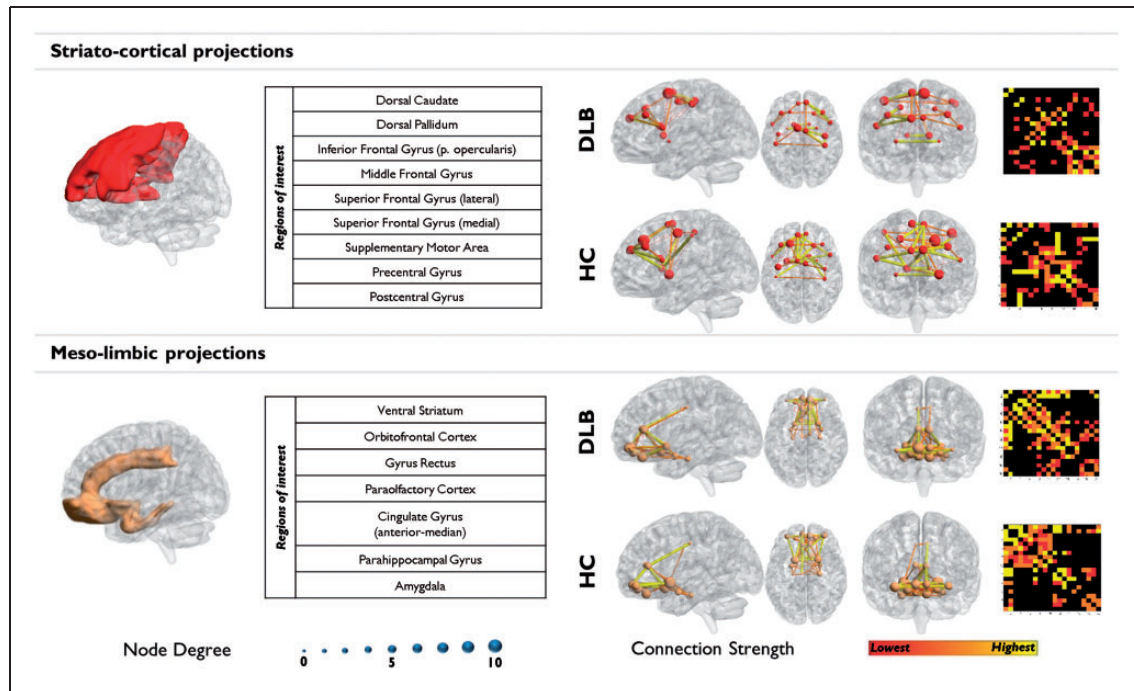All differences were statistically significant ($p < 0.00001$).

Discussion

Novel insights about the possible presence of widespread neurodegeneration effects can be provided by the analysis of complex MC brain networks.

[18F]FDG-PET might be considered an effective measure of energy consumption in neurons, and specifically in synapses.[10–12,68] The fundamentals of [18F]FDG-PET are well established and are based on extensively explored molecular mechanisms.[69] With an estimated 25% of the total brain energy use being dedicated to housekeeping function, [18F]FDG-PET signal primarily reflects neural energy consumption related to: resting potentials (15%), action potentials (16%), and synaptic processes (44%).[70] In addition, astrocytes play also a central role in neurometabolic coupling, as supported experimentally by a large body of evidence, which provides a molecular and cellular basis for interpreting data obtained from functional brain imaging studies.[71]

Figure 3. Alpha-synuclein network analysis. Regions affected by α-synuclein at stages one to four. Greater impairment is found in regions corresponding to the earlier stages (i.e. 1–2), consistently with the short disease duration characterizing our sample.

Figure 4. Dopaminergic networks analysis. Cortical and subcortical projections of the two main dopaminergic pathways. The prevalent impairment of the striato-cortical pathway is clearly visible with a huge disruption of functional connections arising from the dorsal striatum. The meso-limbic pathway is relatively spared, even if a general reconfiguration is found.

Therefore, even if neurons are the primary consumer of glucose, glia cells partially contribute to energy consumption,[72] and may contribute to [18F]FDG-PET signal.[68]

All in all, we assume that the [18F]FDG-PET MC alterations we found are mainly due to the neuropathological events affecting DLB synaptic functions, such as neurodegenerative processes,[1] aggregates of α-synuclein at presynapses,[8] neurotransmitters alterations,[18,73] and possibly neuroinflammatory process.[74] Accordingly, many pathological mechanisms in neurodegenerative conditions, such as intracellular oligomers, neurofibrillary tangles, neuronal mitochondria dysfunction, neurotoxic effect of neuroinflammation, calcium channel changes, besides the altered protein deposition, can induce neuronal and synaptic dysfunction captured by [18F]FDG-PET.[9]

This is the first study assessing brain MC in DLB, using graph theory and SICE method. Previous reports investigated functional connectivity in DLB by using fMRI, applying seed-based and independent component analysis (ICA) methods.[23–28] Seed-based analysis relies on an a priori selection of brain regions that are used as seeds to perform correlation analysis.[23,24] For this reason, seed-based studies might suffer by the choice of an a priori limited number of seed regions, preventing a more comprehensive assessment of functional connectivity. The ICA, on the other hand, allows

the assessment of whole-brain resting state networks, which were found altered in DLB.[27,28] All in all, the fMRI studies have provided mixed results, possibly related to the relatively small sample size (ranging from a minimum of 15 to a maximum of 18 subjects), to the variable disease duration, to the clinical heterogeneity characterizing the sample, and to the different techniques used to assess functional connectivity. One of the less consistent finding reported in DLB fMRI connectivity studies concerns the occipital cortex connectivity. For example, a seed-based study showed n decreased functional connectivity between visual cortex and precuneus,[23] whereas Kenny et al.[24] reported no differences in connectivity between primary visual cortex and other regions, that, however, emerged when the same group used the ICA approach.[27]

Following an innovative metabolic and molecular perspective, we investigated the MC in the whole-brain and in anatomically driven networks on the basis of DLB neuropathology, namely, the proposed progressive spreading of α-synuclein pathology,[6,7] and according to the dopaminergic and cholinergic neurotransmission alterations.

Whole-brain analysis

The analysis of whole-brain MC showed a widespread reconfiguration of brain functional architecture in
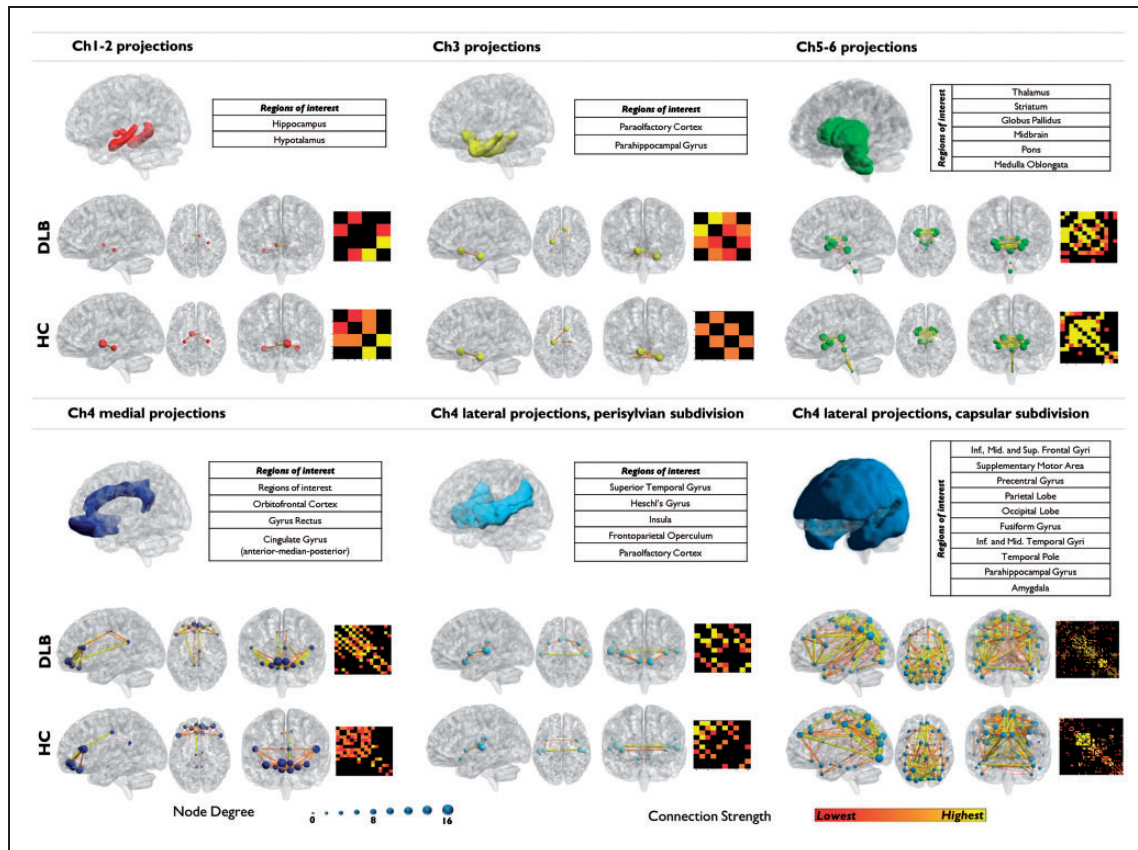
Figure 5. Cholinergic networks analysis. Cortical and subcortical projections of the six main cholinergic pathways. The first row shows regions supplied by Ch1-Ch2 and Ch3 basal forebrain and Ch5-Ch6 brainstem nuclei. The second row shows projections of the three pathways innervating from the nucleus basalis of Meynert (Ch4). Loss of connectivity is observed in regions supplied by Ch1-Ch2 and Ch5–Ch6 nuclei. Ch3 and Ch4 projections displayed variable reconfigurations with altered connectivity profiles.

DLB. Namely, graph theory measures revealed altered connectivity network properties, characterized by a reduction of small-scale and an increase of large-scale connectivity. The resulting imbalance, characterized by decreased segregation and increased integration, reflects a modular dissociation and a consequent functional disorganization of the brain connectome in DLB (Figure 1(a)). The decreased network modularity suggests the presence of functionally less specialized communities of nodes (Figure 2(a)).[65] Connectivity disorganization is also consistent with hub loss, since hubs play a key role in the global organization and efficiency of the brain connectome.[65] In spite of this global reconfiguration, the small-world network organization remained preserved, as previously found in other neurodegenerative diseases.[63,75] The small-worldness, however, is a synthetic index and it may falsely report local integrity, particularly when one of the two reported measures (i.e. segregation and integration) is high enough to compensate for the impairment of the other.[65]

Brain local connectivity

Decreases. A severe disruption of local connectivity was found in the occipital cortex. Occipital lobe dysfunction is associated to simple hallucinations[76] and to the visuo-perceptual deficits observed in DLB.[77]

Cerebellar, thalamic, and brainstem sub-matrices were also affected. Cerebellum is involved in the coordination and temporal organization of various motor and non-motor (e.g. executive and attentional) processes.[78] Recent findings suggest that it may contribute to some neuropsychological features of DLB, such as executive and working memory dysfunctions.[79] Thalamus has a central role in visual perception, attention, and alertness,[80,81] functional domains impaired in DLB.[1] The loss of local connectivity in these structures is compatible with recent models of visual hallucinations, described as the consequence of the combined impairment of both visuo-perceptive and attentional systems.[76] Local connectivity was also reduced in the brainstem, a region widely affected by α-synuclein pathology. Neuronal losses in its neurotransmitters nuclei

were reported in pathological studies of DLB[15,16] and related to the presence of RBD.[82] Moreover, the integrity of brainstem connectivity, in particular of ascending reticular activating system nuclei, is critical for arousal maintenance,[80] which shows fluctuations in DLB.[1]

Increases. Frontal, temporal, parietal, and striatal sub-matrices displayed increased local connectivity. A local reconfiguration, with residual nodes replacing functionally impaired nodes, was found in these regions. This increase in connectivity was reported in other dementia conditions and was related to compensatory mechanisms still possible in early disease phase, such as over-recruitment of partially spared neural function.[22]

Long-range connectivity

Decreases. The analysis of long-range connectivity revealed functional disconnections between occipital, frontal, and cerebellar sub-matrices. Fronto-occipital metabolic and structural abnormalities were previously reported in DLB and related to depressive mood and visual hallucinations.[83,84]

Cerebello-occipital disconnections might explain DLB visual-attentional impairment, given the role of the cerebellum in modulating visual areas activity under attentional demands.[85] The here reported cerebello-frontal disconnection could be part of the cerebello-thalamo-cortical circuit, in which contributes to executive, attentional, and working memory processes.[78] Cerebellar MC was affected at both a small and large-scale level, in accordance to the reported widespread functional, anatomical, and pathological alterations in DLB.[79,86,87] Further studies are necessary to fully disclose the role of the cerebellum in DLB.

Widespread long-range disconnections were crucially found between the thalamus, the superior parietal, occipital, and cingulate cortices. The thalamus is indeed a crucial relé in circuits that are relevant for the motor, cognitive, and behavioral symptoms.[88] Considering the α-syncleopathies, recent fMRI resting state studies reported the involvement of striato-thalamo-cortical in PD.[89]

Increases. The same sub-matrices showing local increases of connectivity also displayed enhanced long-range connectivity, suggesting a more complex reorganization associated with disruption of the functional hierarchy characterizing the normal brain (Figure 1).

Anatomically driven networks

As a main contribution of the present study, we adopted a new prospective to analyze selective vulnerability of MC networks, by targeting well-known molecular and neurotransmission alterations in DLB neuropathology.

The connectivity analysis within networks affected by α-synuclein pathology showed alterations in regions corresponding to α-synuclein Braak stages one to four, with a greater impairment of Braak stages one to two, consistent with the short disease duration characterizing our sample (mean $\pm$ SD = 2.14 $\pm$ 1.4 years) (Figure 3). In particular, medulla oblongata (stage 1), pons (stage 2), and midbrain (stage 3) were characterized by the greatest MC impairment, followed by the impairment in the connected limbic structures (i.e. hippocampal structures, ventral striatum, amygdala), confirming the causal relationship between α-synuclein accumulation and synaptic dysfunction. Our connectomics analysis supports Braak et al.'s[6,7] staging for the spreading of α-synuclein neuropathology in DLB.

The assessment of MC within the dopaminergic networks showed a prevalent impairment of the striato-cortical pathway (Figure 4). The striato-cortical pathway involvement is a hallmark in DLB disease processes, and the substantia nigra is one of the main sites of α-synuclein aggregation.[8] Alpha-synuclein accumulation interferes with neurotransmitter release at presynaptic sites, producing widespread effects on dopaminergic projections.[8] The meso-limbic pathway, assessed here for connectivity integrity, showed preserved functional configuration, consistently with the reported resistance of ventrotegmental area neurons to α-synuclein pathology.[90]

The cholinergic networks also underwent important reconfigurations at different levels (Figure 5). The Ch1-Ch2 and Ch5-Ch6 pathways had the most important reduction in connectivity, possibly suggesting an involvement of these nuclei as an early pathogenic event in DLB. Previous anatomo-pathological studies have shown neuronal loss in these regions,[15,91] and cholinergic impairment was reported in vivo in the subcortical regions they supply.[18]

The cholinergic system has been implicated as potential mechanism in the pathophysiology of visual hallucinations and cognitive fluctuations characterizing DLB.[92] The impairment of Ch5-Ch6 pathway here reported supports its involvement in the pathophysiology of DLB. In particular, the prevalent brainstem-thalamic connectivity impairment is consistent with an involvement of peduncolopontine and thalamic regions in the genesis of visual hallucinations.[93]

Furthermore, the brainstem-thalamic connectivity derangement may be also a fundamental basis in the clinical manifestation of cognitive fluctuations.[81]

Moreover, the involvement of Ch4 projections from the nucleus basalis of Meynert to cortical structures, in particular to the frontal and occipital regions,

is consistent with previous reports.[17,18,94] There is evidence of neuronal loss in nucleus basalis of Meynert and reduction of AchE activity in the neocortical regions supplied by this nucleus, as measured by [11C]-MP4A PET.[14,18,95] The presence of α-synuclein pathology in nucleus basalis of Meynert, in addition to neurodegeneration processes, may contribute to reduction of neocortical cholinergic activity in DLB.[94]

This study has some possible limitations and strengths. The anatomically driven analyses were performed using anatomical regions not specifically constructed for the targeted brain systems. In the future, atlases based on neurotransmitter mapping and/or histopathology may become available, allowing this limitation to be overcome.

It must be acknowledged that in vivo [18F]FDG-PET imaging, although allowing the investigation of molecular and metabolic mechanisms at nanomolar levels, has the limit of spatial resolution. [18F]FDG-PET imaging is a unique tool for in vivo tracking of pathology in humans and future studies combining other microscopic and molecular methods may allow establishing more direct links between metabolic alterations and the underlying cellular and synaptic pathology.

Conclusions

This work focused on DLB at an early disease phase, showing the specific early vulnerability of different networks on a metabolic basis. These results allow for a more comprehensive neuro-functional picture in DLB, paving the way for new research perspectives. For example, assessing the global and local changes in whole-brain functional and molecular networks at later disease phases that could enhance the understanding of DLB progression; the relationship between DLB altered connectivity endophenotype and other synucleinopathies might be a future issue of researches, since diseases sharing the same molecular pathology might present similar vulnerabilities.[2,21] Finally, the future integration of metabolic and functional measures, as provided by combined [18F]FDG-PET and fMRI methods,[34] might provide essential information on the directionality of connections, thus adding knowledge on the altered signaling hierarchies in DLB.

Data used in preparation of this article were obtained from the Alzheimer's Disease Neuroimaging Initiative (ADNI) database (adni.loni.usc.edu). As such, the investigators within the ADNI contributed to the design and implementation of ADNI and/or provided data but did not participate in analysis or writing of this report. A complete listing of ADNI investigators can be found at: http://adni.loni.usc.edu/wp-content/uploads/how_to_apply/ADNI_Acknowledgement_List.pdf.

Authors' contributions

SPC, MT and AS performed analyses and wrote manuscript. LP processed data, SI and GM performed clinical assessments and diagnosis. SFC wrote manuscript. DP designed research and wrote manuscript. All authors reviewed the manuscript.

Supplementary information

Supplementary material for this paper can be found at http://jcbfm.sagepub.com/content/by/supplemental-data

References

1. McKeith IG, Dickson DW, Lowe J, et al. Diagnosis and management of dementia with Lewy bodies: third report of the DLB consortium. *Neurology* 2005; 65: 1863–1872.
2. Cummings JL. Toward a molecular neuropsychiatry of neurodegenerative diseases. *Ann Neurol* 2003; 54: 147–154.
3. Goedert M, Spillantini MG, Del Tredici K, et al. 100 years of Lewy pathology. *Nat Rev Neurol* 2013; 9: 13–24.
4. Volpicelli-Daley L, Luk K and Patel T. Exogenous α-synuclein fibrils induce Lewy body pathology leading to synaptic dysfunction and neuron death. *Neuron* 2011; 72: 57–71.
5. Masuda-Suzukake M, Nonaka T, Hosokawa M, et al. Pathological alpha-synuclein propagates through neural networks. *Acta Neuropathol Commun* 2014; 2: 88.
6. Braak H, Tredici K Del, Rüb U, et al. Staging of brain pathology related to sporadic Parkinson's disease. *Neurobiol Aging* 2003; 24: 197–211.
7. Braak H, Bohl JR, Müller CM, et al. Stanley Fahn lecture 2005: The staging procedure for the inclusion body pathology associated with sporadic Parkinson's disease reconsidered. *Mov Disord* 2006; 21: 2042–2051.
8. Schulz-Schaeffer WJ. The synaptic pathology of α-synuclein aggregation in dementia with Lewy bodies, Parkinson's disease and Parkinson's disease dementia. *Acta Neuropathol* 2010; 120: 131–143.
9. Perani D. FDG-PET and amyloid-PET imaging: the diverging paths. *Curr Opin Neurol* 2014; 27: 405–413.
10. Sokoloff L. Relation between physiological function and energy metabolism in the central nervous system. *J Neurochem* 1977; 29: 13–26.

11. Rocher AB, Chapon F, Blaizot X, et al. Resting-state brain glucose utilization as measured by PET is directly related to regional synaptophysin levels: a study in baboons. *Neuroimage* 2003; 20: 1894–1898.

12. Magistretti PJ, Pellerin L, Rothman DL, et al. Energy on demand. *Science* 1999; 283: 496–497.

13. Kantarci K, Lowe VJ, Boeve BF, et al. Multimodality imaging characteristics of dementia with Lewy bodies. *Neurobiol Aging* 2012; 33: 2091–2105.

14. Lippa CF, Smith TW and Perry E. Dementia with Lewy bodies: choline acetyltransferase parallels nucleus basalis pathology. *J Neural Transm* 1999; 106: 525–535.

15. Schmeichel AM, Buchhalter LC, Low PA, et al. Mesopontine cholinergic neuron involvement in Lewy body dementia and multiple system atrophy. *Neurology* 2008; 70: 368–373.

16. Seidel K, Mahlke J, Siswanto S, et al. The brainstem pathologies of Parkinson's disease and dementia with Lewy bodies. *Brain Pathol* 2014; 25: 121–135.

17. Klein JC, Eggers C, Kalbe E, et al. Neurotransmitter changes in dementia with Lewy bodies and Parkinson disease dementia in vivo. *Neurology* 2010; 74: 885–892.

18. Marcone A, Garibotto V, Moresco RM, et al. [11C]-MP4A PET cholinergic measurements in amnestic mild cognitive impairment, probable Alzheimer's disease, and dementia with Lewy bodies: a Bayesian method and voxel-based analysis. *J Alzheimers Dis* 2012; 31: 387–399.

19. Ballard C, Ziabreva I, Perry R, et al. Differences in neuropathologic characteristics across the Lewy body dementia spectrum. *Neurology* 2006; 67: 1931–1934.

20. Mukaetova-Ladinska EB and McKeith IG. Pathophysiology of synuclein aggregation in Lewy body disease. *Mechanisms of Ageing and Development* 2006; 127: 188–202.

21. Seeley WW, Crawford RK, Zhou J, et al. Neurodegenerative diseases target large-scale human brain networks. *Neuron* 2009; 62: 42–52.

22. Pievani M, Filippini N, van den Heuvel MP, et al. Brain connectivity in neurodegenerative diseases [mdash] from phenotype to proteinopathy. *Nat Rev Neurol* 2014; 10: 620–633.

23. Galvin J, Price J, Yan Z, et al. Resting bold fMRI differentiates dementia with Lewy bodies vs. Alzheimer's disease. *Alzheimer's Dement* 2011; 76: 1797–1893.

24. Kenny ER, Blamire AM, Firbank MJ, et al. Functional connectivity in cortical regions in dementia with Lewy bodies and Alzheimer's disease. *Brain* 2012; 135: 569–581.

25. Kenny ER, O'Brien JT, Firbank MJ, et al. Subcortical connectivity in dementia with Lewy bodies and Alzheimer's disease. *Br J Psychiatry* 2013; 203: 209–214.

26. Franciotti R, Falasca NW, Bonanni L, et al. Default network is not hypoactive in dementia with fluctuating cognition: an Alzheimer disease/dementia with Lewy bodies comparison. *Neurobiol Aging* 2013; 34: 1148–1158.

27. Lowther ER, O'Brien JT, Firbank MJ, et al. Lewy body compared with Alzheimer dementia is associated with decreased functional connectivity in resting state networks. *Psychiatry Res* 2014; 223: 192–201.

28. Peraza LR, Kaiser M, Firbank M, et al. fMRI resting state networks and their association with cognitive fluctuations in dementia with Lewy bodies. *Neuroimage Clin* 2014; 4: 558–565.

29. Morbelli S, Drzezga A, Perneczky R, et al. Resting metabolic connectivity in prodromal Alzheimer's disease. A European Alzheimer Disease Consortium (EADC) project. *Neurobiol Aging* 2012; 33: 2533–2550.

30. Toussaint P-J, Perlbarg V, Bellec P, et al. Resting state FDG-PET functional connectivity as an early biomarker of Alzheimer's disease using conjoint univariate and independent component analyses. *Neuroimage* 2012; 63: 936–946.

31. Titov D, Diehl-Schmid J, Shi K, et al. Metabolic connectivity for differential diagnosis of dementing disorders. *J Cereb Blood Flow Metab*. Epub ahead of print 31 December 2015. DOI: 10.1177/0271678X15622465.

32. Horwitz B, Duara R and Rapoport SI. Intercorrelations of glucose metabolic rates between brain regions: application to healthy males in a state of reduced sensory input. *J Cereb Blood Flow Metab* 1984; 4: 484–499.

33. Passow S, Specht K, Adamsen TC, et al. Default-mode network functional connectivity is closely related to metabolic activity. *Hum Brain Mapp* 2015; 36: 2027–2038.

34. Riedl V, Utz L, Castrillón G, et al. Metabolic connectivity mapping reveals effective connectivity in the resting human brain. *Proc Natl Acad Sci USA* 2015; 113: 428–433.

35. Huang S, Li J, Sun L, et al. Learning brain connectivity of Alzheimer's disease by sparse inverse covariance estimation. *Neuroimage* 2010; 50: 935–949.

36. Lee DS, Kang H, Kim H, et al. Metabolic connectivity by interregional correlation analysis using statistical parametric mapping (SPM) and FDG brain PET; methodological development and patterns of metabolic connectivity in adults. *Eur J Nucl Med Mol Imaging* 2008; 35: 1681–1691.

37. Carbonell F, Charil A, Zijdenbos AP, et al. Hierarchical multivariate covariance analysis of metabolic connectivity. *J Cereb Blood Flow Metab* 2014; 34: 1936–1943.

38. Fornito A, Zalesky A and Breakspear M. The connectomics of brain disorders. *Nat Rev Neurosci* 2015; 16: 159–172.

39. Holtbernd F, Ma Y, Peng S, et al. Dopaminergic correlates of metabolic network activity in Parkinson's disease. *Hum Brain Mapp* 2015; 36: 1–11.

40. Nugent AC, Martinez A, Alfonso AD, et al. The relationship between glucose metabolism, resting-state fMRI BOLD signal, and GABA A -binding potential: a preliminary study in healthy subjects and those with temporal lobe epilepsy. *J Cereb Blood Flow Metab* 2015; 35: 583–591.

41. Perani D, Della Rosa PA, Cerami C, et al. Validation of an optimized SPM procedure for FDG-PET in dementia diagnosis in a clinical setting. *NeuroImage Clin* 2014; 6: 445–454.

42. Perani D, Cerami C, Caminiti SP, et al. Cross-validation of biomarkers to early differential diagnosis and prognosis of dementia in a clinical setting. *Eur J Nucl Med* 2015; 43: 499–508.

43. Varrone A, Asenbaum S, Vander Borght T, et al. EANM procedure guidelines for PET brain imaging using

[18F]FDG, version 2. *Eur J Nucl Med Mol Imaging* 2009; 36: 2103–2110.

44. Riedl V, Bienkowska K, Strobel C, et al. Local activity determines functional connectivity in the resting human brain: a simultaneous FDG-PET/fMRI study. *J Neurosci* 2014; 34: 6260–6266.

45. Della Rosa PA, Cerami C, Gallivanone F, et al. A standardized [(18)F]-FDG-PET template for spatial normalization in statistical parametric mapping of dementia. *Neuroinformatics* 2014; 12: 575–593.

46. Buchert R, Wilke F, Chakrabarti B, et al. Adjusted scaling of FDG positron emission tomography images for statistical evaluation in patients with suspected Alzheimer's disease. *J Neuroimaging* 2005; 15: 348–355.

47. Gallivanone F, Della Rosa P, Perani D, et al. The impact of different 18FDG PET Healthy Subject scans for comparison with single patient in SPM analysis. *Q J Nucl Med Mol imaging* 2014; 50.

48. Dukart J, Mueller K, Horstmann A, et al. Differential effects of global and cerebellar normalization on detection and differentiation of dementia in FDG-PET studies. *Neuroimage* 2010; 49: 1490–1495.

49. Mesulam MM, Mufson EJ, Wainer BH, et al. Central cholinergic pathways in the rat: an overview based on an alternative nomenclature (Ch1-Ch6). *Neuroscience* 1983; 10: 1185–1201.

50. Selden N and Gitelman D. Trajectories of cholinergic pathways within the cerebral hemispheres of the human brain. *Brain* 1998; 121: 2249–2257.

51. Mesulam M. The cholinergic innervation of the human cerebral cortex. *Prog Brain Res* 2004; 145: 67–78.

52. Oades RD and Halliday GM. Ventral tegmental (A10) system: neurobiology. 1. Anatomy and connectivity. *Brain Res Rev* 1987; 12: 117–165.

53. Tziortzi AC, Haber SN, Searle GE, et al. Connectivity-based functional analysis of dopamine release in the striatum using diffusion-weighted MRI and positron emission tomography. *Cereb Cortex* 2014; 24: 1165–1177.

54. Deramecourt V, Bombois S, Maurage CA, et al. Biochemical staging of synucleinopathy and amyloid deposition in dementia with Lewy bodies. *J Neuropathol Exp Neurol* 2006; 65: 278–288.

55. Parkkinen L, Pirttilä T and Alafuzoff I. Applicability of current staging/categorization of alpha-synuclein pathology and their clinical relevance. *Acta Neuropathol* 2008; 115: 399–407.

56. Tzourio-Mazoyer N, Landeau B, Papathanassiou D, et al. Automated anatomical labeling of activations in SPM using a macroscopic anatomical parcellation of the MNI MRI single-subject brain. *Neuroimage* 2002; 15: 273–289.

57. Kroemer NB, Guevara A, Vollstädt-Klein S, et al. Nicotine alters food-cue reactivity via networks extending from the hypothalamus. *Neuropsychopharmacology* 2013; 38: 2307–2314.

58. Tziortzi AC, Searle GE, Tzimopoulou S, et al. Imaging dopamine receptors in humans with [11C]-(+)-PHNO: dissection of D3 signal and anatomy. *Neuroimage* 2011; 54: 264–277.

59. Soret M, Bacharach SL and Buvat I. Partial-Volume Effect in PET Tumor Imaging. *J Nucl Med* 2007; 48: 932–945.

60. Boellaard R. Standards for PET image acquisition and quantitative data analysis. *J Nucl Med* 2009; 50: 11S–20S.

61. Kruschwitz JD, List D, Waller L, et al. GraphVar: a user-friendly toolbox for comprehensive graph analyses of functional brain connectivity. *J Neurosci Methods* 2015; 245: 107–115.

62. Yakushev I, Chételat G and Fischer F. Metabolic and structural connectivity within the default mode network relates to working memory performance in young healthy adults. *Neuroimage* 2013; 79: 184–190.

63. Seo EH, Lee DY, Lee J-M, et al. Whole-brain functional networks in cognitively normal, mild cognitive impairment, and Alzheimer's disease. *PLoS One* 2013; 8: e53922.

64. Xia M, Wang J and He Y. BrainNet Viewer: a network visualization tool for human brain connectomics. *PLoS One* 2013; 8: e68910.

65. Rubinov M and Sporns O. Complex network measures of brain connectivity: uses and interpretations. *Neuroimage* 2010; 52: 1059–69.

66. Friston KJ. Modalities, modes, and models in functional neuroimaging. *Science* 2009; 326: 399–403.

67. Power JD, Schlaggar BL, Lessov-Schlaggar CN, et al. Evidence for Hubs in Human Functional Brain Networks. *Neuron* 2013; 79: 798–813.

68. Lundgaard I, Li B, Xie L, et al. Direct neuronal glucose uptake Heralds activity-dependent increases in cerebral metabolism. *Nat Commun* 2015; 6: 6807.

69. Mosconi L. Glucose metabolism in normal aging and Alzheimer's disease: methodological and physiological considerations for PET studies. *Clin Transl Imaging* 2013; 1: 997–1003.

70. Howarth C, Gleeson P and Attwell D. Updated energy budgets for neural computation in the neocortex and cerebellum. *J Cereb Blood Flow Metab* 2012; 32: 1222–1232.

71. Magistretti PJ. Neuron-glia metabolic coupling and plasticity. *J Exp Biol* 2006; 209: 2304–2311.

72. Lanz B, Gruetter R and Duarte JMN. Metabolic flux and compartmentation analysis in the brain in vivo. *Front Endocrinol (Lausanne)* 2013; 4: 156.

73. Walker Z, Costa DC, Walker RWH, et al. Striatal dopamine transporter in dementia with Lewy bodies and Parkinson disease: a comparison. *Neurology* 2004; 62: 1568–1572.

74. Iannaccone S, Cerami C and Alessio M. In vivo microglia activation in very early dementia with Lewy bodies, comparison with Parkinson's disease. *Park Relat Disord* 2013; 6: 4–9.

75. Göttlich M, Münte TF, Heldmann M, et al. Altered resting state brain networks in Parkinson's disease. *PLoS One* 2013; 8: e77336.

76. Shine JM, O'Callaghan C, Halliday GM, et al. Tricks of the mind: Visual hallucinations as disorders of attention. *Prog Neurobiol* 2014; 116: 58–65.

77. Sanchez-Castaneda C, Rene R, Ramirez-Ruiz B, et al. Frontal and associative visual areas related to visual

hallucinations in dementia with lewy bodies and Parkinson's disease with dementia. *Mov Disord* 2010; 25: 615–622.

78. Balsters JH, Laird AR, Fox PT, et al. Bridging the gap between functional and anatomical features of cortico-cerebellar circuits using meta-analytic connectivity modeling. *Hum Brain Mapp* 2014; 35: 3152–3169.

79. Colloby SJ, O'Brien JT and Taylor J-P. Patterns of cerebellar volume loss in dementia with Lewy bodies and Alzheimer's disease: a VBM-DARTEL study. *Psychiatry Res* 2014; 223: 187–91.

80. Edlow BL, Takahashi E, Wu O, et al. Neuroanatomic connectivity of the human ascending arousal system critical to consciousness and its disorders. *J Neuropathol Exp Neurol* 2013; 71: 531–546.

81. Delli PS, Franciotti R, Taylor J-P, et al. Thalamic involvement in fluctuating cognition in dementia with lewy bodies: magnetic resonance evidences. *Cereb Cortex* 2015; 25: 3682–3689.

82. Boeve BF, Silber MH, Saper CB, et al. Pathophysiology of REM sleep behaviour disorder and relevance to neurodegenerative disease. *Brain* 2007; 130: 2770–2788.

83. Perneczky R, Drzezga A, Boecker H, et al. Right prefrontal hypometabolism predicts delusions in dementia with Lewy bodies. *Neurobiol Aging* 2009; 30: 1420–1429.

84. Kiuchi K, Morikawa M, Taoka T, et al. White matter changes in dementia with Lewy bodies and Alzheimer's disease: a tractography-based study. *J Psychiatr Res* 2011; 45: 1095–1100.

85. Kellermann T, Regenbogen C, De Vos M, et al. Effective connectivity of the human cerebellum during visual attention. *J Neurosci* 2012; 32: 11453–11460.

86. Mori F, Piao Y-S, Hayashi S, et al. Alpha-synuclein accumulates in Purkinje cells in Lewy body disease but not in multiple system atrophy. *J Neuropathol Exp Neurol* 2003; 62: 812–819.

87. Taylor J-P, Colloby SJ, McKeith IG, et al. Covariant perfusion patterns provide clues to the origin of cognitive fluctuations and attentional dysfunction in dementia with Lewy bodies. *Int Psychogeriatr* 2013; 25: 1917–1928.

88. Ziabreva I, Ballard CG, Aarsland D, et al. Lewy body disease: Thalamic cholinergic activity related to dementia and parkinsonism. *Neurobiol Aging* 2006; 27: 433–438.

89. Luo C, Song W, Chen Q, et al. Reduced functional connectivity in early-stage drug-naive Parkinson's disease: a resting-state fMRI study. *Neurobiol Aging* 2014; 35: 431–441.

90. Maingay M, Romero-Ramos M, Carta M, et al. Ventral tegmental area dopamine neurons are resistant to human mutant alpha-synuclein overexpression. *Neurobiol Dis* 2006; 23: 522–532.

91. Fujishiro H, Umegaki H, Isojima D, et al. Depletion of cholinergic neurons in the nucleus of the medial septum and the vertical limb of the diagonal band in dementia with Lewy bodies. *Acta Neuropathol* 2006; 111: 109–114.

92. Ferman TJ, Smith GE, Boeve BF, et al. DLB fluctuations: specific features that reliably differentiate DLB from AD and normal aging. *Neurology* 2004; 62: 181–187.

93. Janzen J, van 't Ent D, Lemstra a W, et al. The pedunculopontine nucleus is related to visual hallucinations in Parkinson's disease: preliminary results of a voxel-based morphometry study. *J Neurol* 2012; 259: 147–154.

94. Tiraboschi P, Hansen L and Alford M. Cholinergic dysfunction in diseases with Lewy bodies. *Neurology* 2000; 54: 25–31.

95. Shimada H, Hirano S, Shinotoh H, et al. Mapping of brain acetylcholinesterase alterations in Lewy body disease by PET. *Neurology* 2009; 73: 273–278.